Video Article

Fabrication of Nanopillar-Based Split Ring Resonators for Displacement Current Mediated Resonances in Terahertz Metamaterials

Chao Liu[1], Joseph Schauff[1], Seokhyeong Lee[1], Jeong-Hyun Cho[1]

[1]Department of Electrical and Computer Engineering, University of Minnesota

Correspondence to: Jeong-Hyun Cho at jcho@umn.edu

URL: https://www.jove.com/video/55289
DOI: doi:10.3791/55289

Keywords: Engineering, Issue 121, metamaterials, terahertz, split ring resonators, displacement current, nanopillar, quality factor, nano gap

Date Published: 3/23/2017

Citation: Liu, C., Schauff, J., Lee, S., Cho, J.H. Fabrication of Nanopillar-Based Split Ring Resonators for Displacement Current Mediated Resonances in Terahertz Metamaterials. *J. Vis. Exp.* (121), e55289, doi:10.3791/55289 (2017).

Abstract

Terahertz (THz) split ring resonator (SRR) metamaterials (MMs) has been studied for gas, chemical, and biomolecular sensing applications because the SRR is not affected by environmental characteristics such as the temperature and pressure surrounding the resonator. Electromagnetic radiation in THz frequencies is biocompatible, which is a critical condition especially for the application of the biomolecular sensing. However, the quality factor (Q-factor) and frequency responses of traditional thin-film based split ring resonator (SRR) MMs are very low, which limits their sensitivities and selectivity as sensors. In this work, novel nanopillar-based SRR MMs, utilizing displacement current, are designed to enhance the Q-factor up to 450, which is around 45 times higher than that of traditional thin-film-based MMs. In addition to the enhanced Q-factor, the nanopillar-based MMs induce a larger frequency shifts (17 times compared to the shift obtained by the traditional thin-film based MMs). Because of the significantly enhanced Q-factors and frequency shifts as well as the property of biocompatible radiation, the THz nanopillar-based SRR are ideal MMs for the development of biomolecular sensors with high sensitivity and selectivity without inducing damage or distortion to biomaterials. A novel fabrication process has been demonstrated to build the nanopillar-based SRRs for displacement current mediated THz MMs. A two-step gold (Au) electroplating process and an atomic layer deposition (ALD) process are used to create sub-10 nm scale gaps between Au nanopillars. Since the ALD process is a conformal coating process, a uniform aluminum oxide (Al_2O_3) layer with nanometer-scale thickness can be achieved. By sequentially electroplating another Au thin film to fill the spaces between Al_2O_3 and Au, a close-packed Au-Al_2O_3-Au structure with nano-scale Al_2O_3 gaps can be fabricated. The size of the nano-gaps can be well defined by precisely controlling the deposition cycles of the ALD process, which has an accuracy of 0.1 nm.

Video Link

The video component of this article can be found at https://www.jove.com/video/55289/

Introduction

Terahertz (THz) metamaterials (MMs) have been developed for biomedical sensors and frequency-agile devices[1,2,3,4,5,6,7,8,9,10,11]. In order to improve the sensitivity and frequency selectivity of the THz MM sensors, a nanopillar-based split ring resonator (SRR) has been designed using displacement current generated inside gold (Au) nanopillar arrays to excite THz resonances with ultra-high quality factors (Q-factors) (~450) (**Figure 1**)[12]. Even though nanopillar-based SRRs show high Q-factors and promising sensing abilities, fabrication of such nanostructures with high aspect ratios (more than 40) and nano-scale gaps (sub-10 nm) over a large area remains challenging[13].

The most commonly used technique to fabricate nano-scale structures is electron-beam lithography (EBL)[14,15,16,17]. However, the resolution of EBL is still limited due to the beam spot size, electron scattering, properties of the resist, and the development process[18,19]. In addition, it is not practical to fabricate nanostructures using EBL over a large area due to a slow process time and large process costs[20]. Another strategy to achieve nanostructures is to use a self-assembly technique[21,22]. By self-assembling metal nanocubes (NCs) in a solution and utilizing the electrostatic interaction and the association of polymer ligands between NCs, a well-organized one-dimensional NC array with nano-scale gaps can be achieved[23]. The nano-gap size depends on the polymer ligands between the NCs and can be controlled by applying different polymer materials with different molecular weights[24,25,26]. Self-assembly is a powerful technique for achieving scalable and cost-efficient nanostructures[23]. However, the fabrication process is more complicated compared to conventional micro and nano fabrication processes, and the control of nano-gap sizes is not precise enough for electronic device applications. In order to successfully fabricate nanopillar-based SRRs, a novel fabrication method should be invented to achieve the following goals: i) the fabrication process is easy to apply and is compatible with conventional micro and nano fabrication processes; ii) fabrication over a large area is applicable; iii) nano-gap sizes can be easily and precisely controlled with a 0.1 nm resolution and can be scaled down to 10 nm or less.

A novel fabrication method is demonstrated using the combination of an electroplating process and an atomic layer deposition (ALD) process to fabricate nanopillar-based SRRs. Since electroplating is a self-filling process with low cost, it is easy to fabricate structures over a large area. ALD is a chemical vapor deposition (CVD) process that can be precisely controlled by the reaction cycle during the process. The resolution of ALD thin film can be 0.1 nm, and the thin film is uniformly coated with a high quality, which is suitable to create nano-scale gaps[27,28]. Nanopillar-based SRR array with 10 nm gaps or less can be successfully fabricated over an area of 6 mm × 6 mm. Both simulated and measured THz

transmission spectra show resonant behaviors with ultra-high Q-factors and large frequency shifts, which proves the feasibility of the nanopillar-based SRRs mediated by displacement current. The detailed fabrication process is described below in the protocol section, and the video protocol can help practitioners to understand the fabrication process and avoid common mistakes associated with the fabrication of nanopillar-based SRRs.

Protocol

Caution: Several of the chemicals used in these syntheses are toxic, highly flammable, and may cause irritation and severe organ damage when touched or inhaled. Please wear appropriate personal protective equipment (PPE) when handling.

1. Preparation of the First Layer of Gold (Au) Nanopillar Arrays (Figure 2a-c and Figure 2e-g)

1. **Preparation of Copper (Cu) Seed layers for Au electroplating (Figure 2a, b and Figure 2e, f)**
    1. Use a 4" high resistivity silicon (Si) wafer (resistivity: 560 - 840 Ω·cm) as the substrate. The Si wafer is N-type doped and polished on one side (**Figure 2a, e**).
    2. Cut the Si wafer into 2 cm × 2.5 cm pieces for later use.
    3. Deposit a 5 nm chromium (Cr) layer on the Si sample using an electron-beam (E-beam) evaporation process as an adhesion layer between the Si and Cu.
    4. Deposit a 10 nm Cu layer on top of the existing Cr layer using an E-beam evaporation process as the seed layer for Au electroplating (**Figure 2b, f**).

2. **Electroplating the Au nanopillar array (Figure 2c, g)**
    1. **Patterning the nanopillar array**
        1. Spin coat photoresist on the sample prepared in section 1.1 at 2,000 rpm for 60 s.
        2. Bake the sample on a hot plate at 115 °C for 60 s.
        3. Expose the photoresist under ultraviolet (UV)-light (power of ~15 mW/cm^2) with a Cr photomask that contains thousands of nanopillar patterns for 22 s.
        4. Develop with a developer for 90 s with agitation.
        5. Rinse the sample with deionized (DI) water and blow-dry the sample with an air gun.
    2. **Electroplating the Au nanopillar array**
        1. Remove the top section of the photoresist on the sample with acetone to expose the Cu seed layer for electrode connection.
        2. Connect the sample (Cu seed layer) to the negative terminal of a source meter using a clamp and a wire. In this case, the sample is the anode during the electroplating process.
        3. Connect a piece of platinum (Pt) coated Si (same size as the sample) to the positive terminal of the source meter. The Pt is the cathode during the electroplating process.
        4. Submerge both the Pt cathode and Cu anode in the Au electroplating solution. Keep the two electrodes facing each other with a distance of ~ 1 cm.
        5. Turn on the source meter and supply a constant voltage of 1.12 V. Electroplate Au on the sample for 8 min (deposition rate: ~ 100 nm/min).
        6. Rinse the sample with DI water, followed by acetone to remove the photoresist.
        7. Rinse the sample with DI water again and blow-dry with an air gun.
        8. Inspect the electroplated Au nanopillar array under a microscope.
        9. Measure the thickness of the Au nanopillars with a profilometer (The thickness of the Au nanopillars is ~800 nm).
        NOTE: Constant current set-up can also be used to electroplate Au nanopillars. In both constant voltage and constant current set-ups, the ideal current and voltage used for Au electroplating can be achieved by trial and error.

2. Creation of Nano-gaps between Au Nanopillars (Figure 2d, h)

1. **Removal of Cr and Cu layers**
    1. Submerge the sample in Cu etchant until the Cu color disappears.
    2. Rinse the sample with DI water and blow-dry with an air gun.
    3. Inspect the Au nanopillars under a microscope.
    4. Submerge the sample in Cr mask etchant for 10 s.
    5. Rinse the sample with DI water and blow-dry with an air gun.
    6. Inspect the Au nanopillars under a microscope.

2. **Fabrication of nano-scale Aluminum Oxide (Al_2O_3) gaps**
    1. Heat the ALD system chamber to 200 °C.
    2. Place the sample in the center of the chamber.
    3. Pump down the chamber to a vacuum and set the cycle number to 100 (deposition rate: ~1 Å/cycle).
    4. Sequentially and alternatively pulse trimethylaluminum (TMA) gas with a time period of 0.015 s and water (H_2O) vapor with a time period of 0.015 s into the chamber to uniformly deposit Al_2O_3 layers on the sample. The time gap between each pulse is 5 s. The chamber pressure during TMA pulse is 10 Torr and the pressure during H_2O vapor pulse is 2 Torr.

5. Purge and vacuum the chamber between each cycle of the deposition. Deposit Al_2O_3 for 100 cycles and take out the sample from the chamber.
6. Measure the thickness of the ALD Al_2O_3 using an ellipsometer.

3. Preparation of the Second Layer of an Au Thin Film (Figure 2i-l and Figure 2m-p)

1. **Preparation of Cu Seed layers for Au electroplating (Figure 2i, m)**
   1. Place the sample in the center of an E-beam evaporator sample holder.
   2. Turn off the rotation of the sample in the E-beam evaporator.
   3. Deposit a 5 nm Cr layer on the sample to act as an adhesion layer between Al_2O_3 and Cu. Use an E-beam evaporation process without sample rotation.
   4. Deposit 10 nm Cu on top of the existing Cr layer using an E-beam evaporation process without sample rotation as the seed layer for Au electroplating.

2. **Electroplating the Au thin film (Figure 2j, n)**
   1. Connect the sample (Cu seed layer) to the negative terminal of the source meter using a clamp and a wire. In this case, the sample is the anode during the electroplating process.
   2. Connect the Pt cathode to the positive terminal of the source meter.
   3. Submerge both the Pt cathode and Cu anode in the Au electroplating solution. Keep the two electrodes facing each other with a distance of ~ 1 cm.
   4. Turn on the source meter and set up constant voltage of 1.35 V and electroplate Au on the sample for 16 min.
   5. Rinse the sample with DI water and blow-dry with an air gun.
   6. Inspect the electroplated Au and the previously electroplated Au nanopillar array under a microscope.
   7. Measure the thickness of the Au nanopillars with a profilometer (Thickness of the Au nanopillars is ~400 nm).
      NOTE: Similar to the Au electroplating in section 1.2.2, constant current set-up can also be used to electroplate Au thin film. In both constant voltage and constant current set-ups, the ideal current and voltage used for Au electroplating can be achieved by trial and error.

3. **Removal of Cr and Cu layers (Figure 2k, o)**
   1. Submerge the sample in Cu etchant for 10 s.
   2. Rinse the sample with DI water and blow-dry with an air gun.
   3. Inspect the Au nanopillars under a microscope.
   4. Submerge the sample in Cr mask etchant for 10 s.
   5. Rinse the sample with DI water and blow-dry with an air gun.
   6. Inspect the Au nanopillars under a microscope.
      NOTE: Alternatively, submerge the sample in Au electroplating solution again to deposit an extra layer of Au on top of the second electroplated Au layer after the removal of Cr and Cu (step 3.3). This extra Au layer increases the total thickness of the second Au layer and ensures good contact between the Au layer and the Al_2O_3 layer (**Figure 2i, p**).

4. Definition of C-shape SRR (Figure 2q-s and Figure 2u-w)

1. **Patterning the C-shape SRR (Figure 2q, u)**
   1. Spin coat a photoresist on the sample at 2,000 rpm for 60 s.
   2. Bake the sample on hot plate of 115 °C for 60 s.
   3. Expose photoresist under UV-light (power of ~15 mW/cm^2) with a Cr photomask for 22 s.
   4. Develop with a developer for 90 s with agitation.
   5. Rinse the sample with DI water and blow-dry the sample with an air gun.

2. **C-shape definition using ion mill (Figure 2r, v and Figure 2s, w)**
   1. Attach the sample on an ion mill sample holder using double-sided Cu conductive tape.
   2. Cool down the ion mill chamber to 6 °C.
   3. Ion mill the sample with a beam voltage of 300 V and a beam current of 125 mA for ~30 min.
   4. Take out the sample and inspect the Au nanopillars outside the C-shape.
   5. Repeat step 4.2.3 and 4.2.4 if Au is still visible outside the C-shape.
   6. Sonicate the sample in acetone to remove the photoresist.
   7. Rinse the sample with DI water and blow-dry with an air gun.
   8. Inspect the sample under a microscope.
   9. Repeat step 4.2.6 and 4.2.7 if photoresist is not fully removed.
      NOTE: Alternatively, apply oxygen resist softening steps to the photoresist before removing the photoresist. However, a sonication bath is the most effective method to remove photoresist if applicable.

5. Removal of Al_2O_3 for Air Nano-gaps (Figure 2t, x)

1. Submerge the sample in 5% hydrogen fluoride (HF) solution for 5 min to remove Al_2O_3.
2. Rinse the sample with DI water and blow-dry with an air gun.

Representative Results

Fabrication schemes show each step (**Figure 2a-x**). Optical images (**Figure 2y-ac**) and scanning electron microscope (SEM) images (**Figure 2ad-ag**) were collected for the nanopillar-based SRRs at different fabrication steps. Animations (**Figure 2a-c**) illustrate the first layer of electroplated Au nanopillars and the second layer of electroplated Au films as well as the nano-gaps created between them. **Figure 2d** shows the cross-section scheme of nanopillar-based SRRs with both Al_2O_3 nano-gaps and air nano-gaps. SEM images were collected for the nanopillar-based SRR array and nano-scale gaps between Au nanopillars (**Figure 2af, 2ag, 3e-h**). Both simulated and measured transmission spectra of the samples with Al_2O_3 nano-gaps and air nano-gaps were shown (**Figure 3i-l**).

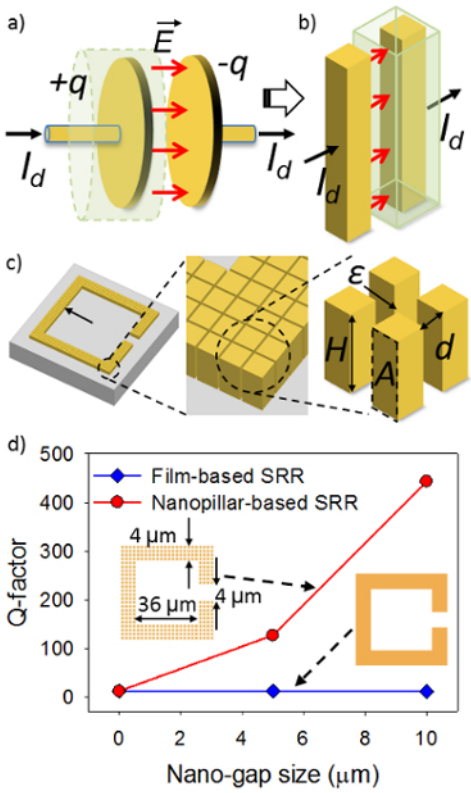

Figure 1: illustration of nanopillar-based SRRs mediated by displacement current. (**a**, **b**) Displacement current (I_d) induced between two metal plates and two nanopillars by electric fields *E*. (**c**) Schematic of nanopillar-based SRRs defined by thousands of Au nanopillars (*H*: height of the nanopillar, *A*: facing area; *d*: nano-gap size; *l*: width of nanopillar and *ε*: permittivity in the nano-gaps). (**d**) Q-factor of thin-film-based SRR and nanopillar-based SRR. A Q-factor of around 450 can be achieved with a nanopillar-based SRR with a nano-gap size of 10 nm. The figure is adapted with permission from Advanced Optical Materials[12]. Please click here to view a larger version of this figure.

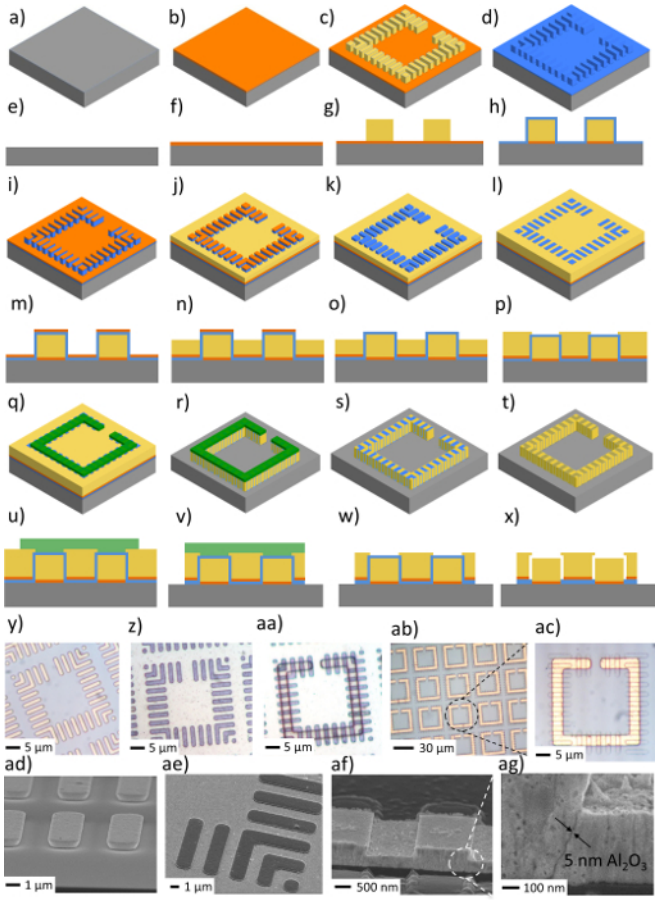

Figure 2: Fabrication schemes of nanopillar-based SRRs. (**a**-**t**) 3D animation and cross-section schematics of the fabrication process of nanopillar-based SRRs. (**y**-**ac**) Optical images of nanopillar-based SRRs at different fabrication steps. (**ad**-**ag**) SEM images of nanopillar-based SRRs at different fabrication steps as well as a 5 nm Al_2O_3 gaps (ag). The figure is adapted with permission from Advanced Optical Materials[12]. Please click here to view a larger version of this figure.

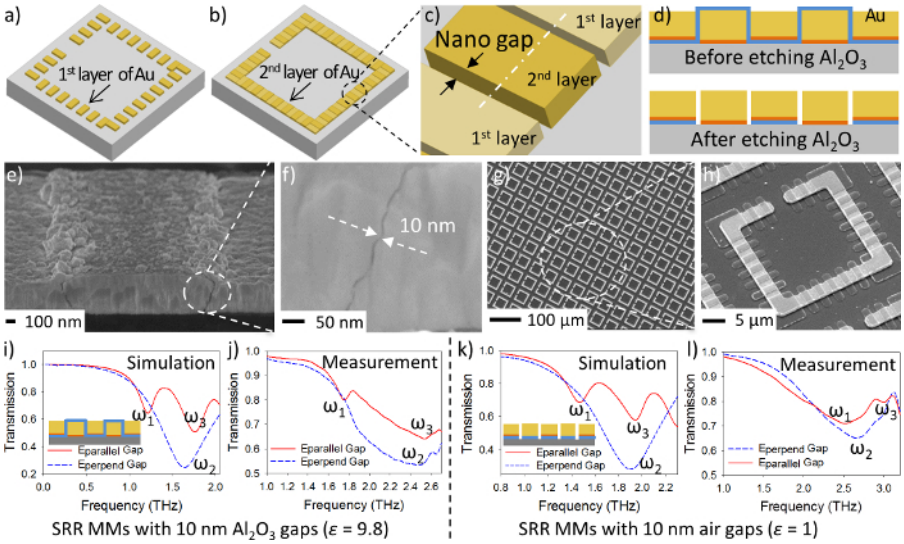

Figure 3: Characterizations of nanopillar-based SRRs. (**a**-**d**) Fabrication schemes of nanopillar-based SRRs. (**e**-**h**) SEM images of nanopillar-based SRRs. (**i**) Simulated transmission spectra of Al_2O_3 nano-gap nanopillar-based SRRs. (**j**) Measured transmission spectra of Al_2O_3 nano-gap nanopillar-based SRRs. (**k**) Simulated transmission spectra of air nano-gap nanopillar-based SRRs. (**l**) Measured transmission spectra of air nano-gap nanopillar-based SRRs. The figure is adapted with permission from Advanced Optical Materials[12]. Please click here to view a larger version of this figure.

Discussion

This fabrication technique has significant advantages for creating nano-scale structures over existing methods such as E-beam lithography and self-assembly. First, nano-scale structures can be realized over a large area (an entire wafer) using a photomask that features nanopillar arrays, which is not practical with an E-beam lithography process. Second, the fabrication process uses a traditional wafer scale micro fabrication process, which is much faster, simpler, and cheaper compared to E-beam lithography. Third, the atomic scale nano-gaps can be easily created by an ALD process with precisely controlled feature sizes.

Cr and Cu E-beam evaporations without sample rotation allow Cr and Cu deposition directly onto the substrate with minimized sidewall deposition. This is crucial for the following Au electroplating process because Au can only be electroplated on the Cu seed layer that is connected to the source meter. Since the Cu layers on top of the Au nanopillars are disconnected with the Cu layer on the substrate, Au cannot be electroplated on the substrate. The quality and thickness of the electroplated Au depend on the electroplating voltage/current and the electroplating time. Higher voltage/current leads to a high deposition rate. However, high voltage/current can also result in low quality Au deposition. Electroplated Au with low quality has a lower electrical conductivity compared to standard Au material as well as lots of voids in Au, which reduces the intensity of the displacement current circulating the SRR, leading to a weak resonant behavior and a lower magnitude of the resonant peaks. Therefore, a suitable voltage/current is essential to achieve high quality Au nanopillars. Electroplating time and voltage/current should be also precisely controlled to make sure that the thickness of the Au thin film (the second layer of Au) is less than that of the Au nanopillars (the first layer of Au).

100 cycles of ALD can achieve about 10 nm thick Al_2O_3 layer on both the Si substrate and the sidewalls of the Au nanopillars. The deposition rate and quality of the Al_2O_3 deposited by ALD depends on the reaction temperature inside the chamber. A reaction temperature of above 200 °C is recommended to achieve high quality Al_2O_3 films. The cycle number and temperature can be precisely controlled to obtain Al_2O_3 layer with desired thickness. The size of the nano-gaps (**Figure 3h**) is critical for achieving high Q-factors of the nanopillar-based SRRs. An increase of nano-gap size increases the energy storage inside the nano-gaps, which leads to a high Q-factor. However the size of nano-gaps cannot be increased without limitation. When nano-gap sizes exceed about 50 nm, the displacement current between Au nanopillars drops dramatically and is unable to pass through the nano-gaps, leading to the disappearance of the resonant responses. In addition, if the size of the Al_2O_3 nano-gaps is less than 2 nm, the electroplating voltage for Au deposition can breakdown the dielectric barrier (Al_2O_3 nano-gaps), resulting in the conduction between Au nanopillars and the Au electroplating solution, which leads to a second Au layer electroplated on top of the Au nanopillars (a first gold layer). This limit leads to the difficulty to achieve ultra-thin Al_2O_3 gaps without breaking the dielectric barrier between Au nanopillars.

A finite element method (FEM) was used to simulate the SRRs (**Figure 3i** and **3k**). Three resonance peaks in the transmission spectra are known as the first (1^{st}) mode, second (2^{nd}) mode, and third (3^{rd}) mode of the SRR. The transmission spectra of the nanopillar-based SRRs with 10 nm Al_2O_3 gaps and 10 nm air gaps were measured using a THz time-domain spectroscopy (**Figure 3j** and **3l**). All the measured transmission spectra match the simulated data, which proves that the fabricated nanopillar-based SRRs meet the expected design.

The combination of continuous metal thin films and dielectric nano-scale gaps provide structures for more energy storage compared to traditional film-based SRRs, which results in ultra-high Q-factors of around 450 (more than 45 times higher than the Q-factor of the traditional thin-film-based SRRs) and large frequency shifts (around 17 times larger than the frequency shift of the thin-film-based SRRs). The unique fabrication technique shown in this video journal allows for the fabrication of thousands of nanopillar forming SRRs over a large area. Since the formation of Au nanopillars largely increases the surface areas of the SRRs and the number of nano-scale gaps between Au nanopillars enhances the amount of the energy storage (electric charges), ultra-high Q-factors can be achieved leading to a high sensitivity. In addition, the substances applied to the nanopillar-based SRRs are presented inside the nano-gaps contribute to the permittivity changes of the nano-gaps, resulting in large frequency shifts of the nanopillar-based SRRs, which leads to a high selectivity. Thus the nanopillar-based SRRs fabricated using Au electroplating and ALD techniques are ideal for highly acute chemical and biomolecular sensing units.

Disclosures

The authors have nothing to disclose.

Acknowledgements

This material is based upon work supported by a start-up fund at the University of Minnesota, Twin Cities. Parts of this work were carried out in the Characterization Facility, University of Minnesota, a member of the NSF-funded Materials Research Facilities Network (www.mrfn.org) via the MRSEC program. A portion of this work was also carried out in the Minnesota Nano Center which receives partial support from the NSF through the NNCI program.

References

1. Xu, X., *et al.* Flexible visible-infrared metamaterials and their applications in highly sensitive chemical and biological sensing. *Nano Lett.* **11** (8), 3232-3238 (2011).
2. Singh, R., Cao, W., Al-Naib, I., Cong, L., Withayachumnankul, W., & Zhang, W. Ultrasensitive terahertz sensing with high-Q Fano resonances in metasurfaces. *Appl. Phys. Lett.* **105** (17), 171101 (2014).
3. Torun, H., Top, F.C., Dundar, G., & Yalcinkaya, A. An antenna-coupled split-ring resonator for biosensing. *J. Appl. Phys.* **116** (12), 124701 (2014).
4. Chen, T., Li, S., & Sun, H. Metamaterials application in sensing. *Sensors.* **12** (3), 2742-2765 (2012).

5. Jaruwongrungsee, K., *et al.* Microfluidic-based Split-Ring-Resonator Sensor for Real-time and Label-free Biosensing. *Procedia Eng.* **120**, 163-166 (2015).
6. Han, J., & Lakhtakia, A. Semiconductor split-ring resonators for thermally tunable terahertz metamaterials. *J. Mod. Optic.* **56** (4), 554-557 (2009).
7. Melik, R., Unal, E., Perkgoz, N.K., Puttlitz, C., & Demir, H.V. Flexible metamaterials for wireless strain sensing. *Appl. Phys. Lett.* **95** (18), 181105 (2009).
8. Naqui, J., Durán-Sindreu, M., & Martín, F. Alignment and position sensors based on split ring resonators. *Sensors.* **12** (9), 11790-11797 (2012).
9. Chiam, S., Singh, R., Gu, J., Han, J., Zhang, W., & Bettiol, A.A. Increased frequency shifts in high aspect ratio terahertz split ring resonators. *Appl. Phys. Lett.* **94** (6), 064102 (2009).
10. Gil, I., *et al.* Varactor-loaded split ring resonators for tunable notch filters at microwave frequencies. *Electron. Lett.* **40** (21), 1347-1348 (2004).
11. Driscoll, T., *et al.* Tuned permeability in terahertz split-ring resonators for devices and sensors. *Appl. Phys. Lett.* **91** (6), 062511 (2007).
12. Liu, C., *et al.* Displacement Current Mediated Resonances in Terahertz Metamaterials. *Adv. Opt. Mater.* **4** (8), 1302-1309 (2016).
13. Huang, M., Zhao, F., Cheng, Y., Xu, N., & Xu, Z. Large area uniform nanostructures fabricated by direct femtosecond laser ablation. *Opt. Express.* **16** (23), 19354-19365 (2008).
14. Broers, A., Molzen, W., Cuomo, J., & Wittels, N. Electron-beam fabrication of 80-Å metal structures. *Appl. Phys. Lett.* **29** (9), 596-598 (1976).
15. Isaacson, M., & Muray, A. Insitu vaporization of very low molecular weight resists using 1/2 nm diameter electron beams. *J. Vac. Sci. Technol.* **19** (4), 1117-1120 (1981).
16. Yang, J.K., *et al.* Understanding of hydrogen silsesquioxane electron resist for sub-5-nm-half-pitch lithography. *J. Vac. Sci. Technol. B.* **27** (6), 2622-2627 (2009).
17. Duan, H., Yang, J.K., & Berggren, K.K. Controlled Collapse of High-Aspect-Ratio Nanostructures. *Small.* **7** (18), 2661-2668 (2011).
18. Cord, B., *et al.* Limiting factors in sub-10nm scanning-electron-beam lithography. *J. Vac. Sci. Technol. B.* **27** (6), 2616-2621 (2009).
19. Manfrinato, V.R., *et al.* Resolution limits of electron-beam lithography toward the atomic scale. *Nano Lett.* **13** (4), 1555-1558 (2013).
20. Ashraf, M., Sreenath, A., & Chollet, F. Low-cost mould for nano-imprinting uses monolayer of self-organized nanospheres. *SPIE Newsroom.* (2007).
21. Hu, T., Gao, Y., Wang, Z., & Tang, Z. One-dimensional self-assembly of inorganic nanoparticles. *Front. Phys. China.* **4**, 487-496 (2009).
22. Kitching, H., Shiers, M.J., Kenyon, A.J., & Parkin, I.P. Self-assembly of metallic nanoparticles into one dimensional arrays. *J. Mater. Chem. A.* **1** (24), 6985-6999 (2013).
23. Klinkova, A., *et al.* Structural and optical properties of self-assembled chains of plasmonic nanocubes. *Nano Lett.* **14** (11), 6314-6321 (2014).
24. Caswell, K., Wilson, J.N., Bunz, U.H., & Murphy, C.J. Preferential end-to-end assembly of gold nanorods by biotin-streptavidin connectors. *J. Am. Chem. Soc.* **125** (46), 13914-13915 (2003).
25. Liu, K., *et al.* Step-growth polymerization of inorganic nanoparticles. *Science.* **329** (5988), 197-200 (2010).
26. Nie, Z., Fava, D., Kumacheva, E., Zou, S., Walker, G.C., & Rubinstein, M. Self-assembly of metal-polymer analogues of amphiphilic triblock copolymers. *Nat. Mater.* **6** (8), 609-614 (2007).
27. Chen, X., *et al.* Atomic layer lithography of wafer-scale nanogap arrays for extreme confinement of electromagnetic waves. *Nat. Commun.* **4** (2361) (2013).
28. Nam, S., *et al.* Sub-10-nm nanochannels by self-sealing and self-limiting atomic layer deposition. *Nano Lett.* **10** (9), 3324-3329 (2010).

